X-band Parallel-Mode and Multifrequency Electron Paramagnetic Resonance Spectroscopy of *S* = 1/2 Bismuth Centers

Julia Haak,[1,2] Julia Krüger,[2,3] Nikolay V. Abrosimov,[4] Christoph Helling,[2,3] Stephan Schulz,[2,3] George E. Cutsail III[1,2*]

[1] Max Planck Institute for Chemical Energy Conversion (CEC), Stiftstraße 34–36, 45470 Mülheim an der Ruhr (Germany)

[2] Institute of Inorganic Chemistry and [3]Center for Nanointegration Duisburg-Essen (CENIDE), University of Duisburg-Essen, Universitätsstraße 5-7, 45141 Essen (Germany)

[4] Leibniz-Institut für Kristallzüchtung, Max-Born Strasse 2, 12489 Berlin (Germany)

*email: george.cutsail@cec.mpg.de

Abstract

The recent successes in the isolation and characterization of several bismuth radicals inspire the development of new spectroscopic approaches for the in-depth analysis of their electronic structure. Electron paramagnetic resonance (EPR) spectroscopy is a powerful tool for the characterization of main group radicals. However, the large electron-nuclear hyperfine interactions of Bi (^{209}Bi, I = 9/2) have presented difficult challenges to fully interpret the spectral properties for some of these radicals. Parallel-mode EPR ($B_1 \parallel B_0$) is almost exclusively employed for the study of $S > 1/2$ systems but becomes feasible for S = 1/2 systems with large hyperfine couplings, offering a distinct EPR spectroscopic method. Herein, we demonstrate the application of conventional X-band parallel-mode EPR for $S = 1/2$, $I = 9/2$ spin systems: Bi doped crystalline silicon (Bi:Si) and the molecular Bi radicals: $[L(X)Ga]_2Bi^{\bullet}$ (X = Cl, I) and $[L(Cl)GaBi(^{Me}cAAC)]^{\bullet+}$ (L = HC[MeCN(2,6-*i*Pr$_2$C$_6$H$_3$)]$_2$). In combination with multifrequency perpendicular-mode EPR (X-, Q-, and W-band frequency), we were able to fully refine both of the anisotropic *g*- and *A*-tensors of these molecular radicals. The parallel-mode EPR experiments demonstrated and discussed here have the potential to enable the characterization of other S = 1/2 systems with large hyperfine couplings, which is often challenging by conventional perpendicular-mode EPR techniques. Considerations pertaining to the choice of microwave frequency are discussed for relevant spin-systems.

Introduction

The recent isolations and characterizations of stable bismuth radicals develop to be an advancing field of curiosity in heavy main group chemistry, not only due to their potential applications in synthesis and catalysis.[1-4] Given that only a handful of stable molecular bismuth radicals has been isolated and characterized thus far,[5-9] general spectroscopic properties and trends within these have yet to be determined. In each case, unique chemical, electronic, or magnetic properties of the bismuth radical influence or dictate what spectroscopic approaches are best suited for their characterization.

Due to their paramagnetic nature, electron paramagnetic resonance (EPR) spectroscopy plays a central role in the characterization of bismuth radicals.[10] For bismuth, a single nuclear active isotope, ^{209}Bi, occurs at 100% natural abundance with a nuclear spin of $I = 9/2$. To date, very few examples of stable bismuth radicals exist and the complete electron paramagnetic characterization of their hyperfine interaction is often challenging. The first stable molecular bismuth radical to be fully characterized by multifrequency EPR was $[O(SiMe_2NAr)_2]Bi^{\bullet}$ (Ar = 2,6-*i*$Pr_2C_6H_3$),[8] which was found to have a very large isotropic hyperfine coupling ($|a_{iso}|$ ~ 3800 MHz), among the largest hyperfine interactions measured yet by EPR spectroscopy.[8] Previously, we have demonstrated the $S = 1/2$ radical behavior of a homoleptically gallium coordinated bismuth radical, $[L(I)Ga]_2Bi^{\bullet}$ (L = HC[C(Me)N(2,6-*i*$Pr_2C_6H_3$)]$_2$), Scheme 1.[9] Variable temperature magnetic susceptibility measurements yielded a response consistent with a $S = 1/2$ and a $g_{av} = 2.05$. The ~4 K perpendicular-mode X-band (~9.6 GHz) EPR spectrum of this radical exhibited numerous broad features from 0 to >7000 G. The higher frequency Q-band (~34 GHz) echo detected EPR failed to resolve distinct *g*-values or components of the anisotropic hyperfine tensor. More recently, we reported the general synthesis and characterization of heteroleptically coordinated group 15 radicals, stabilized by L(X)Ga and a cyclic (alkyl)(amino)carbene (^{Me}cAAC) ligand (^{Me}cAAC = $[H_2C(CMe_2)_2N(2,6\text{-}i\text{-}Pr_2C_6H_3)]C$). Similar to $[L(I)Ga]_2Bi^{\bullet}$, $[L(Cl)GaBi(^{Me}cAAC)]^{\bullet+}$ exhibited a broad perpendicular-mode X-band EPR of numerous transitions.[11] Unfortunately, the determination of accurate EPR parameters from these

previous EPR experiments was not feasible, inspiring the development of additional spectroscopic methods and techniques for the characterization of these unique and complex radicals.

Scheme 1. Molecular Bismuth Radicals $[O(SiMe_2NAr)_2]Bi^{\bullet}$,[8] $[L(X)Ga]_2Bi^{\bullet}$[9,12] and $[L(Cl)GaBi(^{Me}cAAC)]^{\bullet+}$.[11]

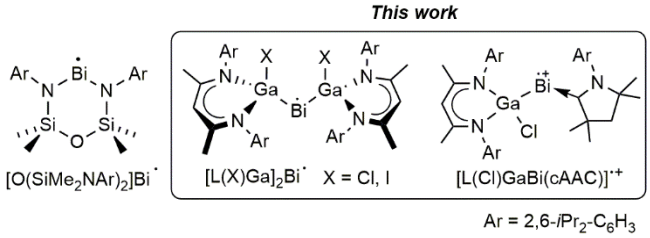

The EPR response of the $S = 1/2$ bismuth radical may be approximated with the classic spin Hamiltonian, $\hat{\mathcal{H}} = \mu_B \mathbf{B}\mathbf{g}\hat{\mathbf{S}} + \hat{\mathbf{S}}\mathbf{A}\hat{\mathbf{I}}$, where the first term is the electronic Zeeman and the second term is the electron-nuclear hyperfine interaction. For the Zeeman interaction, μ_B is the Bohr magneton, **B** is the external magnetic field, and **g** is the electronic **g**-tensor. For the hyperfine interaction, **A** is the hyperfine tensor. At high magnetic fields, where the Zeeman interaction is greater than the hyperfine interaction, the possible spin-states may be described by their quantum numbers $|M_S, M_I\rangle$. The most commonly employed mode of EPR spectroscopy is perpendicular-mode EPR spectroscopy, where the microwave field (B_1) is perpendicular to the magnetic field (B_0): $B_1 \perp B_0$. At the high magnetic field limit, the classic selection rule of $\Delta M_S = 1$, $\Delta M_I = 0$ using 'good' quantum numbers is well obeyed.

For an isotropic $S = 1/2$, $I = 9/2$ spin system, one would observe 10 transitions in the perpendicular-mode EPR experiment. In fact, this is observed for Bi doped crystalline silicon (Bi:Si) recorded at X-band frequency.[13-15] This material is of interest due to its large number of transition states and potential applications in quantum computing.[14-18] The Bi:Si system is well characterized with isotropic $g = 2.0047$ and an isotropic Bi hyperfine coupling of $a_{iso} = 1475.2$ MHz. We do note that the 10-line pattern observed in Bi:Si at X-band frequencies is not equally split as it is in the moderate field limit, where the Zeeman and the hyperfine splittings are closer in energy, hence this field regime will be discussed in more detail shortly. Simply going to higher microwave frequencies, where larger magnetic field strengths are required to observe the resonances, the 10-line pattern will

become evenly spaced because the Zeeman interaction is now sufficiently greater than the hyperfine interaction.

Parallel-mode EPR, $B_1 \parallel B_0$, is possible on common X-band EPR spectrometers with commercially available or home-built microwave cavities[19] (or resonators), where some are 'dual-mode', allowing the spectroscopists to easy select either perpendicular or parallel-mode. Historically, parallel-mode EPR spectroscopy has typically been used to explore $S > 1/2$ systems[20-24] where the zero-field splitting (ZFS) permits admixing of electronic spin-states and observed transitions obey a $\Delta M_S \neq \pm 1$ selection rule (i.e. $\Delta M_S = 0$ or $\Delta M_S = 2$). For the study of $S = 1/2$ centers, parallel-mode EPR has only found very limited applications (if any), as a majority of $S = 1/2$ spin systems, in the high magnetic field limit have no transitions fulfilling the classic '$\Delta M_S \neq \pm 1$' selection rule.

As alluded to earlier, systems with large hyperfine interactions, such as Bi:Si, may not be in the high field limit at conventional microwave frequencies, but in a low or moderate field limit, pushing one to reconsider the classic EPR selection rules. As previously derived for the case of the hydrogen atom by Weil,[25-26] M_S and M_I are not necessarily good quantum numbers in the low or moderate field regimes, but rather spin states should be noted as $|F, M_F\rangle$, the eigenstates of F^2 and F_z of the total angular momentum: $\mathbf{F} = \mathbf{S} + \mathbf{I}$. From this, one may simply rederive the selection rules for both perpendicular- and parallel-mode to be $\Delta M_F = \pm 1$ and $\Delta M_F = 0$, respectively. The $\Delta M_F = 0$ selection rule has curious implications because for $S = 1/2$ systems with large hyperfine coupling at low or moderate fields, this predicts allowed parallel-mode EPR transitions.

Weil initially predicted the allowed transitions for the $S = 1/2$, $I = 1/2$ hydrogen atom (a_{iso} = 1420 MHz), along with their intensities.[25] Later, Mitrikas et al.[27] directly measured both the perpendicular and parallel-mode EPR spectra of the H atom encapsulated in polyhedral oligomeric silsesquioxane cages (^{1}H@h_{72}Q$_8$M$_8$) and observed a hyperfine coupling of A = 1416.58 MHz, in excellent agreement with Weil's proposal. The parallel-mode EPR of the H atom is fairly weak and it is noted that the intensity of both the perpendicular and parallel-mode EPR transitions are determined

by the time dependent perturbation solution of the magnetic dipole transition spin-Hamiltonian operator. Therefore, their intensities have only a magnetic field dependence.[25] Weil proposed that at 2 GHz, the H atom is completely in the low field regime, and the intensities of both the parallel and perpendicular-mode EPR spectra would be comparable, Figure S1. More simply stated, the intensity of the parallel-mode EPR is proportional to the degree of state-mixing, which is greatest in the low field regime. Mitrikas et al.[27] recognized the potential of parallel-mode EPR spectroscopy to other S = 1/2 systems and reported the predicted perpendicular and parallel-mode EPR spectra of Bi:Si.

We first further explored the experimental feasibility of parallel-mode X-band EPR applied to S = 1/2 systems through the study of Bi:Si. The previous challenges we faced characterizing molecular Bi radicals, our successful multi-frequency EPR approaches to other Group 15 radicals, and the prospect of parallel-mode EPR to yield even further insight, inspired us to continue our spectroscopic studies of $[L(I)Ga]_2Bi^{\bullet}$ and $[L(Cl)GaBi(^{Me}cAAC)]^{\bullet+}$. Moreover, the recently isolated $[L(Cl)Ga]_2Bi^{\bullet}$ radical featuring Cl substituents instead of the I substituents of the structurally analogous $[L(I)Ga]_2Bi^{\bullet}$ was included in this study.[12] Together, the parallel-mode and multi-frequency perpendicular-mode EPR spectra offer the most complete characterization of these radicals thus far. Lastly, the application of parallel-mode EPR spectroscopy to S = 1/2 spin systems has rarely been demonstrated thus far, and we will further illustrate the capabilities of conventional EPR spectroscopies, including parallel-mode EPR, to these emerging Bi radical systems and discuss more broadly its application to systems with large hyperfine interactions.

Results and Discussion

The X-band (~9.65 GHz) perpendicular-mode EPR spectrum of Si:Bi exhibited maximum intensity around 25 K. Warming of the sample to temperatures above 40 K yielded weaker signals as expected prior to complete spoiling of the tuning due to a rapid decrease of the observed Q-factor of the cavity. The X-band perpendicular EPR spectrum exhibits ten transitions, following the typical $2I$ + 1 hyperfine splitting pattern. The transitions are of approximately equal intensity but inequivalent

magnetic field spacing. A sharp, more intense transition, is observed at 3429 G, g = 2.0097, and is attributed to non-specific radicals in the Teflon material holding the Si:Bi crystal. The EPR spectrum of the Si:Bi crystal is in excellent agreement with those previously published at X-band frequencies. The Si:Bi perpendicular-mode EPR spectrum exhibits very narrow Gaussian lineshapes that are 3.7 G peak-to-peak, Figure 1. The spectrum is well reproduced by simulation using an isotropic g = 2.0047 and $A(^{209}\text{Bi})$ = 1475.5 MHz, in agreement with the EPR parameters previously reported.[13-15]

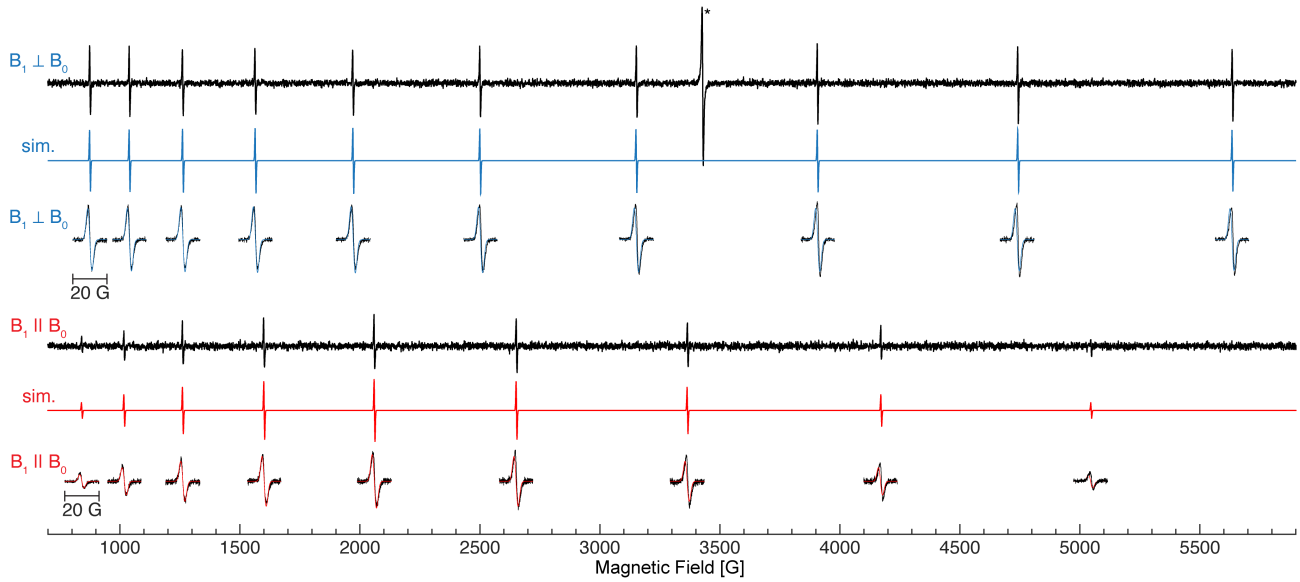

Figure 1. Wide magnetic field X-band perpendicular (~9.65 GHz) and parallel-mode (~9.37 GHz) EPR scans of Si:Bi taken at 25 K. Simulations for each mode are given in color, calculated from the same spin parameters of g = 2.0047 and $A(^{209}\text{Bi})$ = 1475.5 MHz and a 3.7 G (peak-to-peak) linewidth. Narrow magnetic field (20 G) scans are centered at each transition field position. Spectrometer conditions are described in the experimental. The asterisk (*) denotes a g = 2.002 radical impurity.

The parallel-mode X-band (~9.37 GHz) EPR spectrum was also recorded at 25 K, Figure 1. The spectrum exhibits a clear nine-line pattern, one less transition than the perpendicular-mode EPR spectrum. The number of predicted transitions is the result of the $\Delta M_F = 0$ selection rule for parallel-mode EPR, yielding a $2I$ hyperfine splitting pattern, Figure 2. Furthermore, the parallel-mode EPR spectrum exhibits inequivalent transition intensities, with maximum intensity at the 5th and the 6th transitions. Similar to the perpendicular-mode EPR spectrum, the parallel-mode EPR spectrum exhibits transitions that are 3.7 G wide (peak-to-peak). It is important to note that the radical impurity

signal observed at $g = 2$ in the perpendicular-mode EPR spectrum is completely absent in the parallel-mode spectrum as there are no allowed transitions for a $S = 1/2$ with no/weak hyperfine couplings. Simulations of the parallel-mode faithfully reproduce both the transition positions and their intensity patterns, Figure 1.

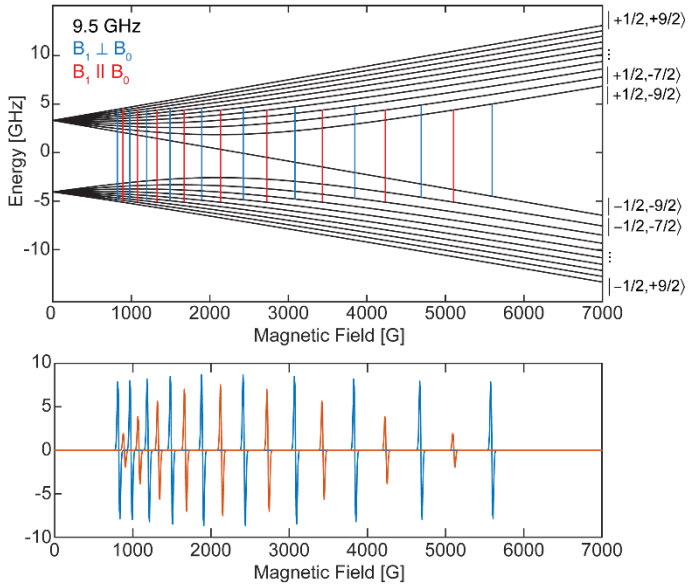

Figure 2. Energy level (Breit-Rabi) diagram of Bi:Si with predicted transitions for parallel and perpendicular mode and the resulting simulated EPR spectrum for a microwave frequency of 9.5 GHz. The transitions are calculated from the isotropic $g = 2.0047$ and $A(^{209}\text{Bi}) = 1475.5$ MHz. Despite M_S and M_I not being good quantum numbers in the low field experiment, the individual levels are labeled with this notation, $|M_S,M_I\rangle$ for ease of reading.

For the Si:Bi system, the EPR spectrum is collected at moderate field limit as the hyperfine features observed in both EPR detection modes are inequivalently spaced. The parallel-mode EPR spectrum of Si:Bi exhibits a less intense spectrum compared to the perpendicular-mode EPR spectrum. Weil previously described the parallel-mode EPR transition intensity mechanism of the hydrogen atom, and showed that the intensity of the parallel-mode transitions decreases as one leaves the low field limit and moves towards the high field limit and the degree of spin-state mixing decreases. Simulations of the Si:Bi parallel-mode EPR response intensity as a function of microwave frequency predicts a constant decrease of intensity away from the maximum response at approximately 7.5 GHz, Figure S2. Therefore, the decreased intensity of the parallel-mode spectrum, due to decreased state-mixing in the moderate field regime at ~9.5 GHz, is a foreseeable phenomenon. One would predict

approximately equally intense perpendicular and parallel-mode EPR spectra at field strengths required for an ~8 GHz EPR experiment. These results immediately demonstrate the ability and serve as proof-of-concept that parallel-mode EPR spectroscopy of an $S = 1/2$, $I = 9/2$ system is not only feasible, but is easily obtained.

The X-band perpendicular-mode and Q-band EPR spectra of $[L(I)Ga]_2Bi^{\bullet}$ were previously reported, however, were unable to offer a complete interpretation of the experiment at the time.[9] The breadth of the EPR spectra, along with magnetic susceptibility measurements, supported the $S = 1/2$ radical structure and localization of the electron to the bismuth center. As a result of long-term cryostorage at 77 K of the previously prepared X-band EPR sample, acquirement of the parallel-mode X-band EPR spectrum was possible, Figure 3. This spectrum offers complementary information to the perpendicular-mode spectrum. Furthermore, the more recently isolated and characterized $[L(Cl)Ga]_2Bi^{\bullet}$ radical was prepared for multifrequency and multi-mode EPR experiments, including a newly prepared W-band EPR sample.[12] $[L(Cl)Ga]_2Bi^{\bullet}$ and $[L(I)Ga]_2Bi^{\bullet}$ exhibit similar X-band perpendicular and parallel-mode EPR spectra (Figure S3) due to their similar electronic structure and the innocence of the gallium coordinated halide. The innocence of these distant atoms to the central radical electronic structure was also previously demonstrated by EPR spectroscopy in the $[L(X)Ga]_2Sb^{\bullet}$ (X = Cl, Br, I) series.[28] Because of the similar electronic structure of the bismuth radical centers in $[L(Cl)Ga]_2Bi^{\bullet}$ and $[L(I)Ga]_2Bi^{\bullet}$, these will simply be referred to as $[L(X)Ga]_2Bi^{\bullet}$.

In addition to the neutral $[L(X)Ga]_2Bi^{\bullet}$ radical, we will present here the EPR spectroscopic characterization of the heteroleptically coordinated bismuth radical cation $[L(Cl)GaBi(^{Me}cAAC)]^{\bullet+}$. The X-band perpendicular-mode EPR spectra of $[L(Cl)GaBi(^{Me}cAAC)]^{\bullet+}$ and $[L(X)Ga]_2Bi^{\bullet}$ exhibit numerous broad transitions extending from 0 to above 7000 G, Figure 3. The X-band perpendicular mode spectrum of $[L(X)Ga]_2Bi^{\bullet}$ exhibits superior signal-to-noise ratio, albeit broad features at high field. The highest field feature at ~6500 G places an upper limit for the evaluation of EPR parameters.

A sharp signal is observed in each sample centered at g~2 that exhibits a different microwave saturation behavior (Figure S4), allowing us to putatively assign this a minor paramagnetic impurity.

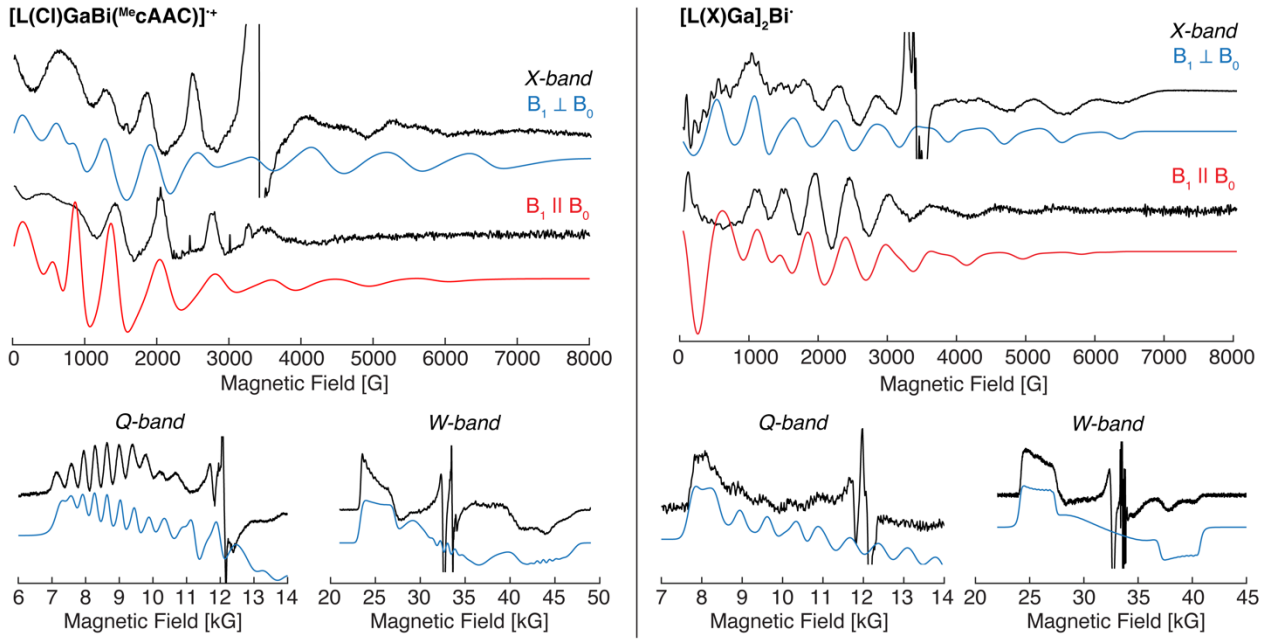

Figure 3. X-band perpendicular ($B_1 \perp B_0$, ~9.63 GHz) and parallel-mode ($B_1 \| B_0$, ~9.33 GHz) EPR spectra in addition to the numerical derivative of two-pulse detected Q-band (~34.0 GHz) and W-band (~94.0 GHz) EPR spectra of $[L(Cl)GaBi(^{Me}cAAC)]^{\bullet+}$ (left) and $[L(X)Ga]_2Bi^{\bullet}$ (right). Simulations for each EPR experiment are given in color, calculated from the same spin parameters for each molecule. $[L(Cl)GaBi(^{Me}cAAC)]^{\bullet+}$: $\mathbf{g}$ = [2.67, 1.95, 1.54]; $\mathbf{A}$ = [1450, 2140, 1360] MHz; hyperfine strain = [200, 0, 400] MHz; g_2-strain = 0.2. $[L(X)Ga]_2Bi^{\bullet}$: $\mathbf{g}$ = [2.61, 2.09, 1.73]; $\mathbf{A}$ = [1200, 2050, 900] MHz; g-strain = [0.03 .2 .01].

The X-band parallel-mode EPR spectra of the Bi radicals exhibit significant intensity and numerous transitions that are clearly different to those observed in the perpendicular-mode spectra. It is noted that the sharp signal at g~2 in the perpendicular-mode EPR is absent in the parallel-mode EPR spectrum, conclusively demonstrating that its origin is of another paramagnetic species. The same phenomenon is observed in the Si:Bi crystal (Figure 1) described above. The differences between the two microwave modes demonstrate the selection power of the technique to differentiate between S = 1/2 systems *with or without* very large hyperfine couplings.

The pulse detected Q-band (~34 GHz) EPR spectrum of each Bi radical exhibits a broad EPR envelope (Figure S5), beginning at ~7000 G and extending beyond the ~14000 G upper limit of the instrument's magnet. The recorded absorption-like spectrum from the integration of the pulse echo is

converted to the numerical derivative spectrum, Figure 3. For [L(Cl)GaBi(^{Me}cAAC)]$^{\bullet+}$, at the low field side of the Q-band EPR spectrum, hyperfine splitting from the Bi nuclei is well-resolved, corresponding to a hyperfine coupling of A_1(^{209}Bi) = 1450 MHz. The spectrum also exhibits a sharp signal near g~2, the same impurity observed in the X-band perpendicular-mode EPR spectrum. The Q-band spectrum, while broad in the absorption, does not offer a distinct g_2 turning point. Lastly, estimates of g_3 and A_3 are unattainable from the Q-band spectrum as they appear to extend well past the high field limit of the instrument's magnet. Well resolved hyperfine at the low field edge of the Q-band spectrum is not observed for [L(X)Ga]$_2$Bi$^{\bullet}$. Rather, the broad feature sets correlated limits for g_1 and A_1.

The higher frequency echo detected W-band (~94.00 GHz) EPR spectrum (Figure S6) affords additional resolution of the g-values and the larger 8 T magnet range of the instrument allows for measurement of the g_3 feature in each Bi radical species. The derivative of the echo detected EPR spectra of [L(Cl)GaBi(^{Me}cAAC)]$^{\bullet+}$ and [L(X)Ga]$_2$Bi$^{\bullet}$ clearly exhibit a low field feature with corresponding g_1 values of 2.67 and 2.61, respectively, Figure 3. The g_1 feature in each spectrum exhibits a square-like broadening due to the Bi hyperfine splitting. However, this hyperfine splitting is not as well resolved as seen in the Q-band spectrum, possibly due to microwave induced strain.[29] In agreement with the Q-band spectrum, the g_1 feature of [L(Cl)GaBi(^{Me}cAAC)]$^{\bullet+}$ is well simulated with a hyperfine coupling of A_1(^{209}Bi) = 1450 MHz. For [L(X)Ga]$_2$Bi$^{\bullet}$ this coupling reduces to A_1(^{209}Bi) = 1200 MHz. At the high field position of the W-band spectra, the g_3 features are distinguished and exhibit broader line shapes than observed for g_1. [L(X)Ga]$_2$Bi$^{\bullet}$ has a larger g_3 value, 1.76, than [L(Cl)GaBi(^{Me}cAAC)]$^{\bullet+}$, 1.56. Lastly, the W-band echo detected EPR spectra offer no clear g_2 position, similar to the Q-band echo detected spectra. However, we do note that the sharper features centered near g = 2.05 and 2.00 are attributed to copper and manganese backgrounds from the W-band cavity (Figure S8). We speculate that possible unfavorable relaxation behavior of the radical such as extremely anisotropic relaxation may yield distorted intensities in the pulsed detected EPR spectra. In

both the Q- and W-band measurements, phase memory times (measured along g_1 and/or g_3) were extremely short (<50 μs). Employment of longer repetition rates increased the relative intensity of responses that are characteristic for copper and manganese background signals (Figure S7-8). Our attempts to measure CW W-band EPR spectra were fruitless.

By simulation of the W-band spectrum, the positions of g_1 and g_3, and their respective widths due to hyperfine splitting are satisfactorily reproduced, Figure 3. Inclusion of a g_2 at the center of the EPR spectra with hyperfine splittings up to 2500 MHz does not influence the other turning points of the W-band spectrum. However, the Q-band spectrum sets an upper limit of the hyperfine coupling, otherwise the low field edge of the spectrum would appear to *even lower* magnetic field. These estimates from the higher frequency EPR spectra may be used with the remaining X-band perpendicular and parallel-mode EPR data to further refine EPR parameters, particularly g_2 and A_2. Employing the EPR parameters resolved from the Q- and W-band experiments (g_1, g_3, A_1, A_3), simulation of both the perpendicular and parallel-mode EPR with values of $g_2 \sim 1.95$ and $A_2 = 2140$ MHz for [L(Cl)GaBi(^{Me}cAAC)]$^{\bullet+}$ and $g_2 = 2.09$ and $A_2 = 2050$ MHz for [L(X)Ga]$_2$Bi$^{\bullet}$ yield spectra that match and align the experiment well.

Similar relative patterns for the perpendicular and parallel-mode transitions are observed in the Breit-Rabi energy diagrams for along each of the molecular/conical *g* directions (Figure 4). The numerical calculation of the Breit-Rabi diagrams does however demonstrate the complexity of the Bi radical spectrum with both large **g** and **A** anisotropies. Here, a single unique solution to the X-band spectra would not be possible without the parameter restraints imposed from the higher frequency Q- and W-band measurements. In the range of 1000 to 3000 G of the X-band perpendicular and parallel-mode EPR spectra, the sharpest features are observed. Additionally, these features exhibit the largest shifts in field relative to one another depending on the mode of the experiment. Inspection of the Breit-Rabi diagrams also shows the largest field position differences for individual transitions of the two microwave modes along the molecular *y* (g_2) direction. This analysis further supports that these

shifting features observed in the experimental spectra are indeed the A_2 hyperfine transitions, not well-observed at higher microwave frequencies.

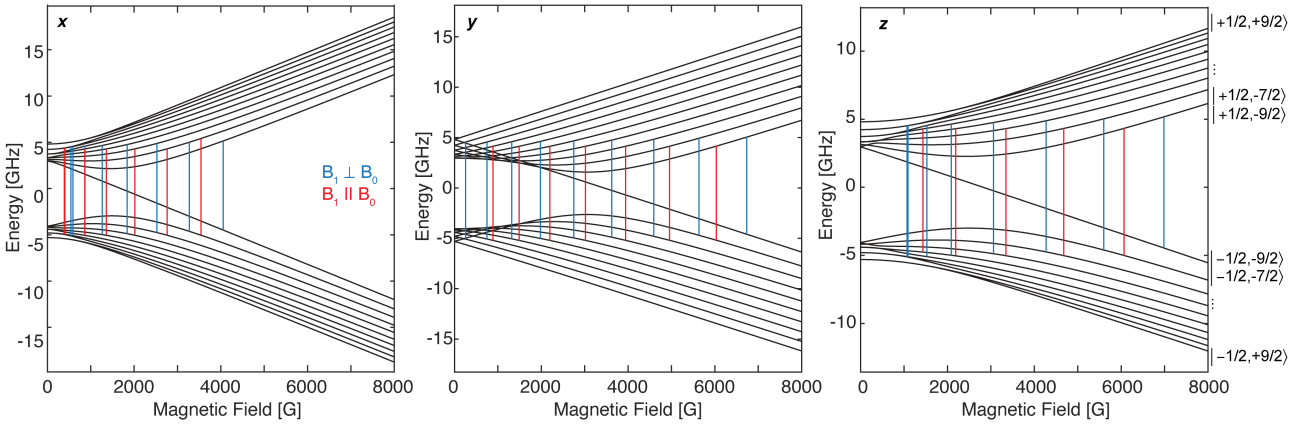

Figure 4. Energy level (Breit-Rabi) diagram of [L(Cl)GaBi(^{Me}cAAC)]$^{\bullet+}$ along the conical molecular axes, *x*, *y* and *z*, aligning with g_1, g_2, and g_3, respectively. The predicted transitions are calculated from full **g**- and **A**(Bi)-tensors detailed in the caption of Figure 3. Both the perpendicular-mode ($B_1 \perp B_0$, ~9.63 GHz) and parallel-mode ($B_1 \parallel B_0$, ~9.34 GHz) EPR transitions are calculated at their experimental frequencies and marked by the vertical bars. Despite M_S and M_I not being good quantum numbers in the low field experiment, the individual levels are labeled with this notation, $|M_S,M_I\rangle$ for ease of reading.

Table 1. Summarized EPR simulation parameters for [O(SiMe$_2$NAr)$_2$]Bi$^{\bullet}$[8], [L(Cl)GaBi(^{Me}cAAC)]$^{\bullet+}$ and [L(X)Ga]$_2$Bi•.

	g = [g_1 g_2 g_3]	**A**(^{209}Bi) = [A_1 A_2 A_3] (MHz)	
[O(SiMe$_2$NAr)$_2$]Bi$^{\bullet}$	[1.832, 1.676, 1.621]	[3830, 2804, 4764]	Ref.[8]
[L(Cl)GaBi(^{Me}cAAC)]$^{\bullet+}$	[2.67, 1.95, 1.54]	[1450, 2140, 1360]	***This work***
[L(X)Ga]$_2$Bi•	[2.61, 2.09, 1.73]	[1200, 2050, 900]	***This work***

Besides the previously characterized [O(SiMe$_2$NAr)$_2$]Bi$^{\bullet}$, [L(Cl)GaBi(^{Me}cAAC)]$^{\bullet+}$ and [L(X)Ga]$_2$Bi$^{\bullet}$ now represent the only stable mononuclear bismuth radicals characterized by EPR spectroscopy. It is apparent that the electronic structure of [O(SiMe$_2$NAr)$_2$]Bi$^{\bullet}$ is quite different from the gallium coordinated Bi radicals studied here, Table 1. It is notable that for [O(SiMe$_2$NAr)$_2$]Bi$^{\bullet}$ each value of the *g*-tensor is less than g_e, differing from both bismuth radicals studied here. The large *g*-anisotropy observed for [L(Cl)GaBi(^{Me}cAAC)]$^{\bullet+}$ and [L(X)Ga]$_2$Bi$^{\bullet}$ is not unlike that observed for the lighter Sb analogues, however, the low g_3 value is unprecedented for a Bi radical and more broadly, Group 15 radicals.[10] The hyperfine of [L(Cl)GaBi(^{Me}cAAC)]$^{\bullet+}$ and [L(X)Ga]$_2$Bi$^{\bullet}$ is significantly smaller than that observed for [O(SiMe$_2$NAr)$_2$]Bi$^{\bullet}$.[8] It may be reasoned that the electropositive Ga

ligands facilitate increased electron delocalization compared to the [O(SiMe$_2$NAr)$_2$] ligand, that coordinates *via* the lighter and more electronegative nitrogen atoms. Supported by previous DFT calculations,[9-11] the radicals [L(Cl)GaBi(^{Me}cAAC)]$^{\bullet+}$ and [L(X)Ga]$_2$Bi$^{\bullet}$ have been previously described as p-orbital centered Bi radicals. Studies in analogous Ga-substituted Sb radicals evidence minimal isotropic spin density, as supported by small isotropic hyperfine couplings.[9-10,30] The large isotropic hyperfine coupling constant of ^{209}Bi, a_0 ~ 77,500 MHz, means that very minor differences in isotropic spin density will profoundly modulate the isotropic hyperfine coupling. For [O(SiMe$_2$NAr)$_2$]Bi$^{\bullet}$, this estimates a Bi s orbital spin density of ~0.05. For [L(Cl)GaBi(^{Me}cAAC)]$^{\bullet+}$ and [L(X)Ga]$_2$Bi$^{\bullet}$, a_{iso} can be estimated in the range of +220 to +1650 MHz depending on the signs of the hyperfine components[9-10], corresponding to isotropic spin density estimates of ~0 to 0.02. This vanishingly small isotropic spin density is consistent with the p-orbital centered radical assignment. Although we do not make any absolute sign assignments for these Bi radicals, it is clear the degree of isotropic spin density is overall very small, and smaller than in [O(SiMe$_2$NAr)$_2$]Bi$^{\bullet}$.

In terms of the experiment feasibility, the choice of microwave frequency is very important. We have already discussed that the parallel-mode EPR transition intensities will depend on the amount of state-mixing. Also, the scale of the hyperfine interaction or the choice of the microwave energy does directly impact the ability to detect the numerous allowed transitions. Working at X-band frequency, we are able to observe all of the possible transitions for Bi:Si, even though this at moderate fields and with inequivalent spacing of the transitions, Figure 5. Higher Q-band frequency begins to approach the high field limit and retains all available transitions. This is the same case for [L(Cl)GaBi(^{Me}cAAC)]$^{\bullet+}$ and [L(X)Ga]$_2$Bi$^{\bullet}$ with similar hyperfine values. For [O(SiMe$_2$NAr)$_2$]Bi$^{\bullet}$, which has a much larger hyperfine coupling, all ten transitions are observable at Q-band frequency. However, at X-band frequency, the number of allowed transitions decreases because the microwave energy is not sufficiently large to meet the $\Delta M_F = 1$ selection rule, or the classic $\Delta M_S = 1$, $\Delta M_I = 0$ selection rule. The only transitions in this low field regime involve the uncoupled-state $|10\rangle$, $|9\rangle \leftrightarrow |10\rangle$

and |10⟩↔|11⟩, Figure 5.[14] These two transitions, labeled in Figure 5 for the case of a_{iso} = 3800 MHz at X-band frequencies, correspond to |9⟩↔|10⟩ ≡ |-1/2, -7/2⟩↔|-1/2, -9/2⟩ with only a flip of the nuclear spin, and |10⟩↔|11⟩ ≡ |-1/2,-9/2⟩↔|+1/2,-9/2⟩ corresponding to only a flip of the electron spin. Both cases obey the $\Delta M_F = 1$ selection rule, making them observable in perpendicular X-band EPR spectroscopy. This is why Schwamm et al. observed an X-band EPR spectrum of relatively few transitions, but numerous transitions in the Q-band experiment.[8] We do refer the interested reader to relevant qubit studies of Bi:Si and proposals of utilizing level |10⟩ as an initial-state rather than the ground-state.[14] For EPR spectroscopic characterization, employing an EPR spectrometer with increased microwave frequency at the moderate field limit to better match the total angular momentum (**F** = **S** + **I**) energies will facilitate the observation of all possible allowed transitions in both perpendicular and parallel-mode EPR spectroscopy.

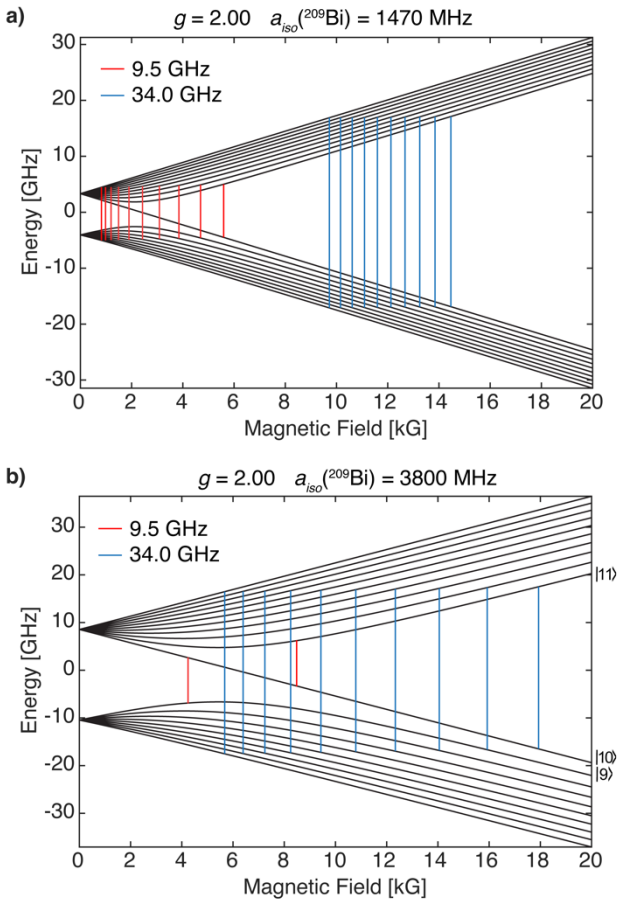

Figure 5. Breit-Rabi energy level diagrams with approximate multifrequency perpendicular-mode EPR transitions for (a) Bi:Si and (b) $[O(SiMe_2NAr)_2]Bi^{\bullet}$. An isotropic **g** and **A** is used for simple

representation of the multifrequency differences anticipated for $[O(SiMe_2NAr)_2]Bi^{\bullet}$. The energy levels $|9\rangle$, $|10\rangle$,$|11\rangle$ are labeled in (b) without quantum numbers.

Conclusion

We have demonstrated the ability of parallel-mode EPR spectroscopy to offer complementary information to the more common perpendicular-mode EPR experiment for $S = 1/2$ systems of large hyperfine coupling. With this new approach, we report the full EPR characterization of $[L(Cl)GaBi(^{Me}cAAC)]^{\bullet+}$ and $[L(X)Ga]_2Bi^{\bullet}$ by conventional EPR laboratory techniques. While multifrequency EPR experiments serve to refine and offer excellent spectral information, the ability to collect dual-mode information on a single laboratory instrument for such complex systems is both attractive and advantageous to EPR spectroscopists. The commercial availability of dual-mode cavities and ease of the experiment presented here has an unmistakable appeal. High frequency EPR spectroscopy, above that demonstrated here, still has excellent potential in the characterization of these bismuth radicals with large hyperfine coupling. Such high frequency techniques have, with high resolution, characterized other $S = 1/2$ systems possessing extreme hyperfine, such as Lu(II) center with an isotropic hyperfine coupling of 3467 MHz.[31] Furthermore, the ability of parallel-mode EPR to be applied to an $S = 1/2$ spin system is a fairly novel application of the technique and warrants further considerations in other complex spin $S = 1/2$ systems. One may envision the development of new or the modification of current low-frequency and broadband EPR spectrometers[32] to perform parallel-mode EPR spectroscopy for $S = 1/2$ with large hyperfine couplings.

Materials and Methods

Bismuth doped silicon

Single float-zone crystals of bismuth doped silicon were made at the Leibniz-Institut für Kristallzüchtung (Berlin, Germany). The final crystal sizes were 2 x 2 x 4 mm and were made of natural abundance Si with a Bi doping of 3.4×10^{15} cm^{-3}. The crystals were loaded into the EPR

spectrometer and held fixed to the bottom end of a quartz EPR tube by a minimal length of Teflon shrink tubing, covering approximately 1.5 mm of the top of the crystal.

Molecular Bi Radicals

Previously prepared[9] X-band EPR samples of $[L(I)Ga]_2Bi^{\bullet}$ (10 mM in toluene) were recovered from long-term cryostorage (77 K) for new measurements. $[L(Cl)GaBi(^{Me}cAAC)]^{\bullet+}$ and $[L(Cl)Ga]_2Bi^{\bullet}$ were synthesized as previously described[11-12] and samples for EPR spectroscopy were prepared anaerobically as 10 mM solution in fluorobenzene ($[L(Cl)GaBi(^{Me}cAAC)]^{\bullet+}$) or 5 mM solution in toluene ($[L(Cl)Ga]_2Bi^{\bullet}$) and frozen in custom 0.9 mm (W-band), 2.8 mm (Q-band) and 4 mm (X-band) OD quartz EPR tubes.

EPR Spectroscopy

Continuous-wave (CW) X-band EPR spectra were measured on a Bruker E500 spectrometer equipped with an Oxford liquid helium flow cryostat. Spectra were collected in a dual-mode X-band resonator, operated in either perpendicular-mode (TE_{102}) or parallel-mode (TE_{012}).

The CW X-band EPR spectra on the Si:Bi sample were collected at ~25 K in perpendicular- (~9.65 GHz) and parallel- (~9.37 GHz) mode with 100 kHz and 1 G field modulation and the following parameters: full width spectra: time constant = 20.48 ms, sweep time = 671 s, number of points = 8192, number of scans = 4 and 12 for perpendicular- and parallel-mode, respectively. Spectra of each individual transition: time constant = 81.92 ms, sweep time = 168 s, number of points = 512, number of scans = 2 and 5 to 13 for perpendicular- and parallel-mode, respectively.

CW X-band EPR spectra of the molecular Bi radicals were measured at ~4 K in perpendicular- (~9.63 GHz) and parallel-mode (~9.33 GHz ($[L(X)Ga]_2Bi^{\bullet}$), ~9.34 GHz ($[L(Cl)GaBi(^{Me}cAAC)]^{\bullet+}$)) with the following parameters: field modulation frequency = 100 kHz, field modulation amplitude = 6 G, time constant = 81.92 ms, sweep time = 336 s, number of points = 4096. For spectra in perpendicular-mode 1 ($[L(X)Ga]_2Bi^{\bullet}$) and 6 scans ($[L(Cl)GaBi(^{Me}cAAC)]^{\bullet+}$) were collected, respectively. For spectra in parallel-mode 10 ($[L(Cl)Ga]_2Bi^{\bullet}$), 4 ($[L(I)Ga]_2Bi^{\bullet}$) and 20 scans

([L(Cl)GaBi(^{Me}cAAC)]$^{\bullet+}$) were collected. The spectra of [L(Cl)GaBi(^{Me}cAAC)]$^{\bullet+}$ at several microwave powers (Figure S4) were obtained under the same conditions, but with 1024 points and sweep times of 168 s, respectively.

Q-band (~33.98 GHz ([L(Cl)GaBi(^{Me}cAAC)]$^{\bullet+}$), ~34.02 GHz ([L(Cl)Ga]$_2$Bi$^{\bullet}$)) pulsed EPR spectra were collected on a Bruker Elexsys E580 spectrometer equipped with a home-built up/down Q-band pulse conversion accessory,[33] a cylindrical TE_{011} microwave resonator[34] and an Oxford CF935 helium flow cryostat and temperature controller. The spectra were obtained with a two-pulse Hahn sequence ($\pi/2$–τ–π–τ–echo) with the following parameters: For [L(Cl)GaBi(^{Me}cAAC)]$^{\bullet+}$: temperature: 6 K, π = 80 ns, repetition rate = 300 us, shots per point = 25, number of points = 4096, τ was varied between 300 and 650 ns and the respective spectra summed with 3 scans for each value. For [L(Cl)Ga]$_2$Bi$^{\bullet}$: temperature: 7 K, π = 32 ns, repetition rate = 250 us, shots per point = 250, number of points = 8192, τ was varied between 300 and 600 ns and the respective spectra summed with 1 scans for each value.

W-band (~94.00 GHz ([L(Cl)GaBi(^{Me}cAAC)]$^{\bullet+}$), ~94.04 GHz ([L(Cl)Ga]$_2$Bi$^{\bullet}$)) pulsed EPR measurements of were collected on a Bruker Elexsys E680 spectrometer with closed cycle helium cryostat system at 6 K ([L(Cl)GaBi(^{Me}cAAC)]$^{\bullet+}$) and 10 K ([L(Cl)Ga]$_2$Bi$^{\bullet}$), respectively. The spectra were collected with a two-pulse Hahn sequence ($\pi/2$–τ–π–τ–echo), applying the following parameters: π = 40 ns, repetition rate = 500 us, shots per point = 1024, number of points = 5200, τ was varied between 300 and 600 ns and the respective spectra summed. The magnet was swept up and down at the same sweep rate for each τ value and the offsets averaged to account for sweep delays.

All energy level diagrams, transitions and EPR simulations were performed in Matlab with the EasySpin (v 6.0.0) package.

Acknowledgements

The authors thank Dr. Leonid Rapatskiy for technical assistance. The authors thank the Max Planck Society (G.E.C), Evonik Industry (doctoral fellowship C. H.) and the DFG (SCHU 1069/23-2, S.S.) for financial support.

References

1. Lichtenberg, C., Molecular bismuth(III) monocations: structure, bonding, reactivity, and catalysis. *ChemComm* **2021**, *57* (37), 4483-4495. DOI: 10.1039/d1cc01284c
2. Lichtenberg, C., Well-Defined, Mononuclear Bi^{I} and Bi^{II} Compounds: Towards Transition-Metal-Like Behavior. *Angew. Chem. Int. Ed. 55* (2), 484-486. DOI: 10.1002/anie.201509234
3. Helling, C.; Schulz, S., Long-Lived Radicals of the Heavier Group 15 Elements Arsenic, Antimony, and Bismuth. *Eur. J. Inorg. Chem.* **2020**, *2020* (34), 3209-3221. DOI: 10.1002/ejic.202000571
4. Lichtenberg, C., Radical Compounds of Antimony and Bismuth. In *Encyclopedia of Inorganic and Bioinorganic Chemistry*, 2020; pp 1-12.
5. Ishida, S.; Hirakawa, F.; Furukawa, K.; Yoza, K.; Iwamoto, T., Persistent Antimony- and Bismuth-Centered Radicals in Solution. *Angew. Chem. Int. Ed.* **2014**, *53* (42), 11172-11176. DOI: 10.1002/anie.201405509
6. Ishida, S.; Hirakawa, F.; Iwamoto, T., A Series of Two-Coordinate Group-15 Element (P, As, Sb, Bi) Centered Radicals Having Bulky Alkyl Groups. *B. Chem. Soc. Jpn.* **2018**, *91* (7), 1168-1175. DOI: 10.1246/bcsj.20180057
7. Weinert, H. M.; Wolper, C.; Haak, J.; Cutsail III, G. E.; Schulz, S., Synthesis, structure and bonding nature of heavy dipnictene radical anions. *Chem. Sci.* **2021**, *12* (42), 14024-14032. DOI: 10.1039/d1sc04230k
8. Schwamm, R. J.; Harmer, J. R.; Lein, M.; Fitchett, C. M.; Granville, S.; Coles, M. P., Isolation and Characterization of a Bismuth(II) Radical. *Angew. Chem. Int. Ed.* **2015**, *54* (36), 10630-10633. DOI: 10.1002/anie.201504632
9. Ganesamoorthy, C.; Helling, C.; Wolper, C.; Frank, W.; Bill, E.; Cutsail III, G. E.; Schulz, S., From stable Sb- and Bi-centered radicals to a compound with a Ga=Sb double bond. *Nat. Comm.* **2018**, *9* (1), 87. DOI: 10.1038/s41467-017-02581-2
10. Cutsail III, G. E., Applications of electron paramagnetic resonance spectroscopy to heavy main-group radicals. *Dalton Trans.* **2020**, *49* (35), 12128-12135. DOI: 10.1039/d0dt02436h
11. Krüger, J.; Haak, J.; Wölper, C.; Haberhauer, G.; Schulz, S., Single Electron Oxidation of Carbene-Coordinated Pnictinidenes – Entry into Heteroleptic Radical Cations and Metalloid Clusters. **2022**, Submitted.
12. Krüger, J.; Wölper, C.; Schulz, S., Stepwise Bi–Bi Bond Formation: From a Bi-centered Radical to Bi_4 Butterfly and Bi_8 Cuneane-Type Clusters. *Inrog. Chem.* **2020**, *59* (15), 11142-11151. DOI: 10.1021/acs.inorgchem.0c01657
13. Feher, G., Electron Spin Resonance Experiments on Donors in Silicon. I. Electronic Structure of Donors by the Electron Nuclear Double Resonance Technique. *Phys. Rev.* **1959**, *114* (5), 1219-1244. DOI: 10.1103/physrev.114.1219
14. Mohammady, M. H.; Morley, G. W.; Monteiro, T. S., Bismuth Qubits in Silicon: The Role of EPR Cancellation Resonances. *Phys. Rev. Lett.* **2010**, *105* (6), 067601-067604. DOI: 10.1103/physrevlett.105.067602
15. Pica, G.; Wolfowicz, G.; Urdampilleta, M.; Thewalt, M. L. W.; Riemann, H.; Abrosimov, N. V.; Becker, P.; Pohl, H.-J.; Morton, J. J. L.; Bhatt, R. N.; Lyon, S. A.; Lovett, B. W., Hyperfine Stark effect of shallow donors in silicon. *Phys. Rev. B* **2014**, *90* (19), 195204. DOI: 10.1103/physrevb.90.195204
16. Mortemousque, P. A.; Berger, S.; Sekiguchi, T.; Culan, C.; Elliman, R. G.; Itoh, K. M., Hyperfine clock transitions of bismuth donors in silicon detected by spin-dependent recombination. *Phys. Rev. B* **2014**, *89* (15), 161-110. DOI: 10.1103/physrevb.89.155202
17. Mohammady, M. H.; Morley, G. W.; Nazir, A.; Monteiro, T. S., Analysis of quantum coherence in bismuth-doped silicon: A system of strongly coupled spin qubits. *Phys. Rev. B* **2012**, *85* (9), 094404-094416. DOI: 10.1103/physrevb.85.094404
18. Morley, G. W.; Warner, M.; Stoneham, A. M.; Greenland, P. T.; Tol, J. v.; Kay, C. W. M.; Aeppli, G., The initialization and manipulation of quantum information stored in silicon by bismuth dopants. *Nat. Mater.* **2010**, *9* (9), 725-729. DOI: 10.1038/nmat2828

19. Petasis, D. T.; Hendrich, M. P., A new Q-band EPR probe for quantitative studies of even electron metalloproteins. *J. Magn. Reson.* **1999**, *136* (2), 200-206. DOI: 10.1006/jmre.1998.1657
20. Hendrich, M. P.; Debrunner, P. G., Electron-Paramagnetic-Res Spectra of Quintet Ferrous Myoglobin and a Model Heme Compound. *J. Magn. Reson.* **1988**, *78* (1), 133-141. DOI: 10.1016/0022-2364(88)90163-1
21. Hendrich, M. P.; Debrunner, P. G., Integer-Spin Electron-Paramagnetic Resonance of Iron Proteins. *Biophys J* **1989**, *56* (3), 489-506. DOI: 10.1016/S0006-3495(89)82696-7
22. Pierce, B. S.; Elgren, T. E.; Hendrich, M. P., Mechanistic implications for the formation of the diiron cluster in ribonucleotide reductase provided by quantitative EPR spectroscopy. *J. Am. Chem. Soc.* **2003**, *125* (29), 8748-8759. DOI: 10.1021/ja021290h
23. Marts, A. R.; Greer, S. M.; Whitehead, D. R.; Woodruff, T. M.; Breece, R. M.; Shim, S. W.; Oseback, S. N.; Papish, E. T.; Jacobsen, F. E.; Cohen, S. M.; Tierney, D. L., Dual Mode EPR Studies of a Kramers ion: High-Spin Co(II) in 4-, 5-and 6-Coordination. *Appl. Magn. Reson.* **2011**, *40* (4), 501-511. DOI: 10.1007/s00723-011-0225-5
24. Piligkos, S.; Collison, D.; Oganesyan, V. S.; Rajaraman, G.; Timco, G. A.; Thomson, A. J.; Winpenny, R. E. P.; McInnes, E. J. L., Single-crystal parallel-mode EPR spectroscopy of an *S*=6 ground-state transition-metal cluster. *Phys. Rev. B* **2004**, *69* (13), 134424. DOI: 10.1103/physrevb.69.134424
25. Weil, J. A., The hydrogen atom, revisited: Parallel-field magnetic resonance. *Concepts Magn. Res. A* **2006**, *28A* (5), 331-336. DOI: 10.1002/cmr.a.20062
26. Weil, J. A.; Bolton, J. R., *Electron paramagnetic resonance: elementary theory and practical applications*. 2nd ed.; Wiley-Interscience: Hoboken, N.J., 2007.
27. Mitrikas, G.; Sanakis, Y.; Ioannidis, N., Parallel-Mode EPR of Atomic Hydrogen Encapsulated in POSS Cages. *Appl. Magn. Reson.* **2020**, *51* (11), 1451-1466. DOI: 10.1007/s00723-020-01263-5
28. Helling, C.; Wolper, C.; Cutsail III, G. E.; Haberhauer, G.; Schulz, S., A Mechanistic Study on Reactions of Group 13 Diyls LM with Cp*SbX_2-From Stibanyl Radicals to Antimony Hydrides. *Chem. Eur. J.* **2020**, *26* (59), 13390-13399. DOI: 10.1002/chem.202001739
29. Hagen, W. R.; Albracht, S. P. J., Analysis of Strain-Induced EPR-Line Shapes and Anisotropic Spin-Lattice Relaxation in a [2Fe-2S] Ferredoxin. *Biochim. Biophys. Acta* **1982**, *702* (1), 61-71. DOI: 10.1016/0167-4838(82)90027-9
30. Helling, C.; Cutsail III, G. E.; Weinert, H.; Woelper, C.; Schulz, S., Ligand Effects on the Electronic Structure of Heteroleptic Antimony-Centered Radicals. *Angew. Chem. Int. Ed.* **2020**, *59* (19), 7561-7568. DOI: 10.1002/anie.202000586
31. Kundu, K.; White, J. R. K.; Moehring, S. A.; Yu, J. M.; Ziller, J. W.; Furche, F.; Evans, W. J.; Hill, S. Clock Transition Due to a Record 1240 G Hyperfine Interaction in a Lu(II) Molecular Spin Qubit 2021.
32. Hagen, W. R., Very Low-Frequency Broadband Electron Paramagnetic Resonance Spectroscopy of Metalloproteins. *J. Phys. Chem. C* **2021**, *125* (15), 3208-3218. DOI: 10.1021/acs.jpca.1c01217
33. Judd, M.; Jolley, G.; Suter, D.; Cox, N.; Savitsky, A., Dielectric Coupler for General Purpose Q-Band EPR Cavity. *Appl. Magn. Reson.* **2021**. DOI: 10.1007/s00723-021-01404-4
34. Reijerse, E.; Lendzian, F.; Isaacson, R.; Lubitz, W., A tunable general purpose Q-band resonator for CW and pulse EPR/ENDOR experiments with large sample access and optical excitation. *J. Magn. Reson.* **2012**, *214* (1), 237-243. DOI: 10.1016/j.jmr.2011.11.011